Multimodal Technologies and Interaction

MDPI

Article

A Wearable Bidirectional Human–Machine Interface: Merging Motion Capture and Vibrotactile Feedback in a Wireless Bracelet

Julian Kindel [1,†], Daniel Andreas [1,*,†], Zhongshi Hou [1], Anany Dwivedi [2] and Philipp Beckerle [1,3]

[1] Chair of Autonomous Systems and Mechatronics, Friedrich-Alexander-Universität Erlangen-Nürnberg, 91054 Erlangen, Germany; philipp.beckerle@fau.de (P.B.)
[2] Artificial Intelligence (AI) Institute, Division of Health, Engineering, Computing and Science, University of Waikato, Hamilton 3216, New Zealand; anany.dwivedi.fau@gmail.com
[3] Department of Artificial Intelligence in Biomedical Engineering, Friedrich-Alexander-Universität Erlangen-Nürnberg, 91054 Erlangen, Germany
* Correspondence: daniel.andreas@fau.de
† These authors contributed equally to this work.

Abstract: Humans interact with the environment through a variety of senses. Touch in particular contributes to a sense of presence, enhancing perceptual experiences, and establishing causal relations between events. Many human–machine interfaces only allow for one-way communication, which does not do justice to the complexity of the interaction. To address this, we developed a bidirectional human–machine interface featuring a bracelet equipped with linear resonant actuators, controlled via a Robot Operating System (ROS) program, to simulate haptic feedback. Further, the wireless interface includes a motion sensor and a sensor to quantify the tightness of the bracelet. Our functional experiments, which compared stimulation with three and five intensity levels, respectively, were performed by four healthy participants in their twenties and thirties. The participants achieved an average accuracy of 88% estimating three vibration intensity levels. While the estimation accuracy for five intensity levels was only 67%, the results indicated a good performance in perceiving relative vibration changes with an accuracy of 82%. The proposed haptic feedback bracelet will facilitate research investigating the benefits of bidirectional human–machine interfaces and the perception of vibrotactile feedback in general by closing the gap for a versatile device that can provide high-density user feedback in combination with sensors for intent detection.

Keywords: haptic feedback; human–machine interfaces; wireless communication; prototyping

Citation: Kindel, J.; Andreas, D.; Hou, Z.; Dwivedi, A.; Beckerle, P. A Wearable Bidirectional Human–Machine Interface: Merging Motion Capture and Vibrotactile Feedback in a Wireless Bracelet. *Multimodal Technol. Interact.* **2024**, *8*, 44. https://doi.org/10.3390/mti8060044

Academic Editors: Mu-Chun Su and Sven Mayer

Received: 1 March 2024
Revised: 7 May 2024
Accepted: 21 May 2024
Published: 23 May 2024

1. Introduction

Humans interact with their environment through sensory feedback, including vision, hearing, touch, smell, and taste. The sense of touch in particular plays a crucial role in proprioception, allowing for individuals to sense movement, action, and location of limbs [1], thereby contributing to a sense of presence within their environment. More reliable sensory signals have a greater impact on perceptual experiences, resulting in a nuanced understanding of the world and the establishment of causal relations between events [2]. Haptic feedback plays a vital role in enhancing tactile interactions across various devices and applications ranging from mobile phones to advanced robotic devices, as well as virtual and augmented reality applications. It directly influences the user by varying the intensity, location, or pattern of feedback to reflect the dynamics or general state of the interaction. Sensory feedback can be applied to a variety of applications, improving the interaction of robotic or virtual limbs with the environment or providing information about any generic machine that is controlled by a user.

A common application of sensory feedback, for instance, is to help to develop a feeling for the force exerted on an object by an actuator such as simulating increasing grasping forces in virtual or robotic hands through intensified vibration feedback. This

allows for improved control, making tasks such as grasping and lifting fragile objects safer, as the user can better assess the force exerted by them on the object. Additionally, the need for visual attention decreases as the movements of the virtual or robotic limb can be registered through haptic feedback by itself or in addition. This leads to lower cognitive loads for users, allowing for them to accomplish the tasks with higher precision and ease, as shown in a recent study by Thomas et al. [3], who examined an improvement in neural efficiency when using haptic-shared control for myoelectric prostheses. The results of another study suggest that both sensory and motor inputs play an equal role in shaping the representation of spatial body coordinates, and these coordinates are susceptible to multisensory enhancing effects [4]. Furthermore, the use of sensory feedback specifically in an upper limb prosthesis has been shown to reduce phantom limb pain in amputees [5] and increase confidence in the prosthesis [6], thereby enhancing acceptance for its use.

Haptic feedback can be realized by stimulating tactile sensations to convey information about the environment to the user. This extends and complements the communication between human and machine, beyond visual or auditory perception to create a more immersive experience for the user. The largest organ of the human body is the skin, which contains various types of receptors responsible for different perceptions. There are various types of mechanoreceptors [7,8] that are responsible for detecting tactile stimuli. These receptors work together to enable a variety of tactile sensations and send information about the environment to the central nervous system. The behavior of the different receptors is important to understand to design more effective haptic feedback devices of the future.

1.1. Related Work

This work focuses on non-invasive haptic feedback which ensures connecting the feedback device to the user without the need for a medical intervention. This can make the device more accessible to the user by eliminating a potential barrier that could arise from the fear of invasive measures. Non-invasive haptic feedback devices can be easily replaced or upgraded with technological advancements, ensuring the feedback system stays current without necessitating medical intervention for users. There are different approaches to haptic feedback, which differ primarily in the type of actuators used and thus also in the stimulated receptors described below.

Thermal feedback involves perceiving haptic sensations through thermoreceptors. This can be implemented by Peltier elements in wristbands, for instance [9]. However, due to the relatively slow response time for temperature changes resulting from the Peltier effect, it may be less suitable for rapid and dynamic feedback.

Electrotactile feedback makes use of small electric currents to stimulate nerves underneath the skin. Due to its interference with electromyography signals [10], it is, however, less suitable as a feedback device for myoelectric prostheses, for instance.

Mechanotactile feedback activates mechanoreceptors by applying direct force to the user's skin [10], with Merkel cells primarily detecting pressure on the skin and Ruffini corpuscles sensing the resulting skin deformation or stretching [8,11]. This force can be generated by diverse actuators, like digital servo motors controllable in individual steps. When combined with a mechanical structure, these actuators enable adjustable pressure or skin deformation. Antfolk et al. [12] used five servo motors with a lever at the end of which a round contact point is attached for a tactile feedback system. This allowed force and pressure to be exerted via the motor. Each of the motors, placed on the forearm, was intended to represent pressure on a specific fingertip. Pressure can also be generated through piezoelectric thick-film vibrators [13], where a change in length is induced perpendicular to the skin. These actuators are based on the inverse piezoelectric effect, in which a change in the length of the piezoelectric crystal can be induced by applying voltage [13]. A rapid change in voltage, e.g., due to a high-frequency square wave, leads to a rapid contraction and expansion of the piezoelectric crystal, causing the actuator to vibrate. This allows the application of both vibration and pressure simultaneously, providing the possibility of bimodal haptic feedback, which has also been attempted in other works [14,15].

Although piezoelectric actuators can stimulate high pressure with a short rise time, they are unsuitable for a wearable device due to the high voltage required [16] and the high costs.

Vibrotactile feedback is commonly used in everyday electronics such as smartphones, game console controllers, or smartwatches. Vibration motors can be easily integrated into products and can provide haptic perception even without direct contact between the actuator and the user [16]. Additionally, they are small, cost-effective, easy to use, and replaceable [10] and are thus often used in human–machine interaction scenarios. Vibrotactile feedback targets specific mechanoreceptors, namely Meissner and Pacinian corpuscles. Meissner corpuscles are located in the uppermost layer of the skin, especially in hairless areas such as fingertips or palms. They are highly sensitive to light touches and vibrations in the range of 10–200 Hz [17,18]. Meissner corpuscles are classified as rapidly adapting receptors, meaning that with constant stimulation, the stimulus transmitted to the nervous system diminishes over time. Pacinian corpuscles, on the other hand, are located in the deeper dermis and are sensitive to vibrations and rapid changes in pressure [8]. Vibrations in the range of 40–800 Hz can be detected, and the bandwidth of 200–300 Hz is particularly suitable for perception of vibrations [17,18].

The most common actuators for vibrotactile feedback are eccentric rotating mass vibration motors and Linear Resonant Actuators (LRA) [16]. In an eccentric rotating mass vibration motor, an asymmetrical mass rotates on the shaft of a Direct Current (DC) motor, generating vibration through the centrifugal force of the mass [16]. Eccentric rotating mass vibration motors are more cost-effective than LRAs and have the advantage that the frequency and amplitude of vibration can be controlled through the amplitude of the input voltage without the need for an additional driver circuit. This, however, does not allow independent control of the frequency and amplitude of vibration, since both increase with the input voltage, which makes targeting specific mechanoreceptors challenging. Bimbo et al. [19], for instance, employed four eccentric rotating mass vibration motors positioned on a bracelet. One bracelet is located on the forearm, and another on the upper arm to provide feedback on touched objects during the control of robotic arms. In this setup, the rotational axis of the motors is parallel to the skin surface.

An LRA motor consists of a spring-mass system excited to oscillate at a specific frequency [16]. When an alternating current is applied to the coil, it generates a magnetic field that interacts with the magnet, causing the mass to move back and forth in a linear motion, thereby producing vibration. Control of an LRA is achieved through the amplitude and frequency of the input voltage. Although LRAs are more expensive, they achieve higher intensities than eccentric rotating mass vibration motors. Furthermore, the amplitude of the LRA's vibration can be controlled independently of the frequency, allowing for it to target specific mechanoreceptors while retaining full control over vibration intensity. Seiler et al. [20] designed a haptic feedback device consisting of two bracelets, each containing four LRAs worn on the upper arm and forearm. Stimuli were applied at eight circumferential angles, with four generated by real actuators, and four by virtual stimuli. The results of the participants showed an almost linear correlation between the angle of the perceived and presented stimulus, showing the potential of phantom sensation to improve spatial resolution for haptic feedback.

Besides making use of the spatial resolution of haptic feedback, the information density transmitted to the user can further be increased by extending the vibration intensity range through the use of particularly strong vibration motors. Unfortunately, especially commercial devices [21,22] often lack information about the specific model of the vibration motors, which makes comparisons concerning vibration intensity range challenging. Further, commercial devices are usually designed with a specific application in mind. While this specialization can be beneficial, it often limits the use to explore new applications thus making these devices less suitable for research applications involving interactions between humans and real or virtual robots. The Myo Armband by Thalmic Labs Inc., Ontario, CA, USA [21], for instance, focuses mostly on intent detection with eight EMG sensors and a nine-axis Inertial Measurement Unit (IMU). The armband contains a single vibration motor, which is only of limited use since it

lacks spatial information and the feedback is only transmitted by altering the duration of the vibration and not the intensity. VibroTac S which was published by the German Aerospace Center [22], on the other hand, is more focused on user feedback and includes six cylindrical vibration motors that can each individually be controlled concerning intensity. However, since the VibroTac S was designed as an assistive device for blind people to provide information about the surroundings by the addition of three distance sensors, it lacks sensors that can be used for intent detection.

While there are various approaches to implementing haptic feedback devices, there is a consistent pattern in the motivation to improve the interaction between humans and machines [14,15,19,21–25]. However, to facilitate research in the field of bidirectional human–machine interfaces, there is a need for a versatile bidirectional device that can provide high-density user feedback in combination with sensors for intent detection such as an IMU.

1.2. Objectives

In this work, we aim to develop a multi-purpose haptic feedback bracelet that allows bidirectional communication. The vibration motors incorporated into the bracelet must provide a high vibration amplitude, offering a broad range of perceptible intensity levels, effectively increasing the amount of information that the user can perceive compared to previous devices. To further enhance the haptic feedback bracelet towards a versatile bidirectional human–machine interface, our objective is to integrate an IMU to gather motion data. While the combination of vibrational feedback with electromyography as well as the combination of vibrational feedback with strain and pressure sensors have already been explored in the past [25–27], there was no work covering the combination of vibrotactile feedback and motion sensors such as an IMU. This additional data have the potential to enhance decoding accuracy for intent detection or to control virtual or robotic limbs directly . Fischer et al. [28] reported a variation in perceived vibration intensity based on the tightness of a haptic feedback bracelet around the arm. To explore this further, we plan to integrate a force sensor into the haptic feedback device, capable of detecting bracelet tightness for each user. This information could be used to study the impact of tightness on perceived vibration intensity and aid in an automatic calibration process to adjust the motor intensity based on how tightly the bracelet is fastened around the arm. Additionally, the force sensor can be used to detect muscle tension when worn, which can be used for intent detection. For seamless integration into existing human–machine interfaces and to enable real-time operation, we use the Robot Operating System (ROS) for the haptic interface. The design will finally be released as open-source to promote accessibility and collaborative development. The technical design of the wireless haptic feedback bracelet is introduced in Section 2, outlining the requirements and challenges of alignment to human anatomy and perception. The proposed device is then tested and evaluated concerning its functionality in Section 3 by four participants estimating three and five different vibration intensity levels. Section 4 then discusses the findings and concludes the results.

2. Design of the Wireless Haptic Feedback Bracelet

The requirements of the human-centered design for the proposed haptic feedback bracelet are based on anatomical aspects, user preferences, and experiences from previous studies on human–machine interfaces. Starting with the anatomical aspects, the bracelet should fit people with different circumferences on the upper arm and forearm. The global average of mid-upper arm circumference of adults is 25.7 ± 4.2 cm [29], while the average dominant forearm circumference values for men and women are 24.2 cm and 20.5 cm, respectively, covering a total range of 16 to 33 cm [30]. To match this wide range in circumference, the bracelet should ideally be elastic for higher comfort during use, and further adjustable in size to fit even the most extreme cases of forearm and upper arm circumferences.

To operate effectively, the vibration motors of the bracelet should precisely target the vibration-sensitive mechanoreceptors, namely Meissner and Pacinian corpuscles, by selecting vibration frequencies in the range of 40 to 200 Hz. For optimal suitability, the device should feature a wearable design, achievable through compact dimensions and wireless communication. The significance of these elements becomes evident in studies examining the factors contributing to the limited acceptance of prostheses among amputees. This issue arises from disparities between user needs and available devices, coupled with dissatisfaction regarding the device's functionality, comfort, and control [31]. Prior research on human–machine interfaces has underscored the significance of low latencies in providing effective tactile feedback. Depending on the task, a system response time ranging from 16 to 60 ms is generally imperceptible to humans, as noted in studies like [32]. Other research suggests that latencies below 100 to 150 ms are satisfactory [33]. Furthermore, it has been observed that users are particularly sensitive to latencies in tactile feedback [32], emphasizing the crucial need for designing responsive feedback devices with minimal processing time.

2.1. Electric Circuit Layout

Figure 1 illustrates a schematic overview of the haptic feedback bracelet design and its components. The design centers around a microcontroller with WiFi capabilities, facilitating communication with other devices. This communication is employed to receive commands related to vibration intensities or to transmit data from the motion sensor. The bracelet incorporates five vibration motors, each commanded by a haptic motor controller connected to the microcontroller via an I2C multiplexer. While the motion sensor is also connected via the I2C multiplexer, the force sensor is directly linked to the microcontroller through an available analog input. For wireless functionality, a battery charging system is integrated between the supply voltage of the USB port and the linear voltage regulator, ensuring the supply of the necessary voltage and current for the components. The serial interface of the USB port allows for rapid programming and debugging of the software. Moreover, it enables the ability to equip the device with a custom-created program via a flash chip, facilitating fast wireless communication with ROS programs.

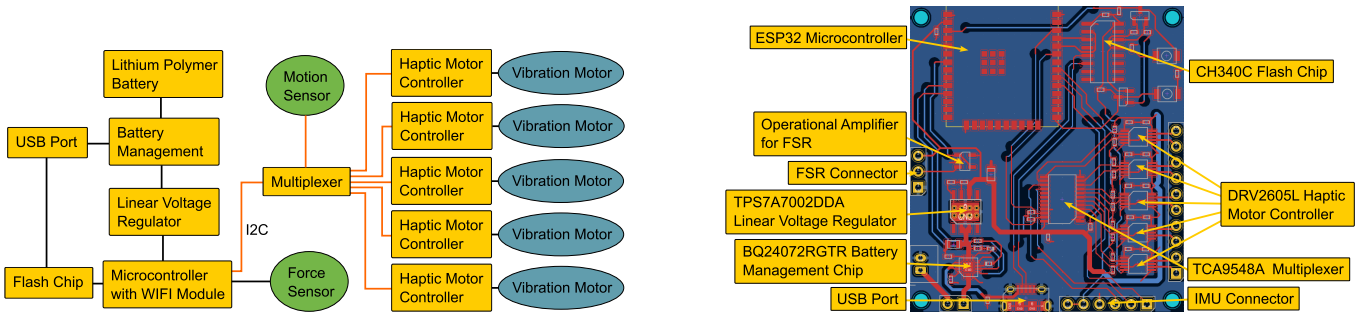

Figure 1. The microcontroller connects to the motion sensor and vibration motors via I2C. The feedback bracelet can communicate through WiFi with other devices, while the lithium polymer battery allows for complete wireless operation. The schematic overview of the device and its components is shown on the left. Components in squares are integrated into the PCB. Components in circles are externally connected. Actuators are marked blue and sensors are green. The annotated design of the PCB on the right shows the position of electrical SMD components as well as connectors for the IMU and FSR.

In designing the Printed Circuit Board (PCB) , which is shown in Figure 1, special emphasis was given to its compactness to ensure comfort during wear. The decision to avoid external breakout boards for components was made to save space, as they often demand more room and may not be optimally tailored to the circuit's specifications, potentially limiting functionality. To achieve this goal, most circuit components were directly integrated

into the PCB using surface-mounted device (SMD) components, effectively minimizing space requirements.

As the microcontroller, an ESP32 from Espressif Systems, Shanghai, China in the form of a WROOM32E module is used, enabling WiFi connectivity thanks to the integrated antenna. It also features a fast processor that allows for parallel processing with its two cores. Utilizing the second core of the ESP32 enables the execution of processes simultaneously, offering the advantage of reducing the processing time for functions and consequently minimizing the overall latency of the haptic feedback device. The force-sensitive resistor (FSR) 402 Short from Interlink Electronics, Camarillo, CA, USA is used to measure the tightness of the bracelet on the user's arm and is connected by the respective pins shown in Figure 1. The sensor allows for force measurements in the range of 0.1 to 10 Newton. To acquire inertial data from the haptic feedback bracelet to improve the control of virtual or robotic limbs for instance, the BNO085 IMU by Bosch Sensortec, Reutlingen, Germany is added to the device through the connection pins as shown in Figure 1. The BNO085 IMU contains a three-axis gyroscope, an accelerometer, and a magnetometer, and it is connected via I2C to the microcontroller. The IMU comes with onboard sensor fusion algorithms to minimize drift and outputs data at a rate of 100 Hz, allowing for responsive control in applications with minimal latency. The ability to control the amplitude of the LRA's vibration independently of the frequency can make the feedback more consistent and allows for targeting specific mechanoreceptors, making LRA the actuator of choice for the proposed haptic feedback device. Various LRAs were compared based on the manufacturer's specifications as in Table 1 and tested within small experiments to find the ideal actuator.

Table 1. Specifications of different Linear Resonant Actuators based on the manufacturer's datasheet (Vybronics, Brooklyn, NY, USA).

Model	Current [mA] avg.	Rise Time to 50% Power	Fall Time to 50% Power	Vibration Force [mN]	Surface Area [mm^2]
VLV101040A	317	10 ms	40 ms	26.97	100
VL120628H	105	40 ms	60 ms	17.65	72
VL91022-160-320H	155	50 ms	60 ms	29.42	203

The lithium polymer battery can provide sufficient power to all three LRA models, accommodating up to five actuators. While it is desirable to minimize latency, as indicated by the rise and fall times to 50% power in Table 1, all three LRA models exhibit reasonable responsiveness. In the context of serving as a feedback device for robotic or virtual limbs, the vibration intensity determined from the applied force from the actuator is expected to rise and fall continuously, which makes the latency of the LRAs less relevant. The higher the maximum vibration force, the easier it should be to distinguish between a certain number of vibration intensities. The VL120628H LRA provides the lowest vibration force, while the intensities of models VLV101040A and VL91022-160-320H are similarly high, which was also evident in initial tests, where each LRA operated at their resonant frequency with maximum intensity. The surface area of the LRAs impacts heat dissipation. While model VLV101040A with the lowest surface area heated up after a few seconds leading to discomfort of the user, no significant heating was observed for the other two models after operating at maximum power for several seconds. Lastly, due to the larger surface area of VL91022-160-320H, the vibration was perceived as more pleasant and was thus chosen for the haptic feedback bracelet. The applied force of the LRA is highest when excited at its resonant frequency, which is at 160 Hz along the vibration axis for VL91022-160-320H. Accordingly, it lies in the range of 40 to 200 Hz and thus targets both Meissner and Pacinian corpuscles, hopefully leading to a better perception of the vibration by the user.

2.2. Software Interface

The software consists of two physically separated programs, running on the ESP32 microcontroller of the haptic feedback bracelet (client) and a master PC with an Ubuntu 20.04 LTS operating system, which connect via WiFi. To ensure broad compatibility, the interface on the Ubuntu machine was programmed using ROS Noetic Ninjemys from Open Robotics. The communication between the ROS interface and the haptic feedback bracelet was implemented using the Transmission Control Protocol (TCP), ensuring reliable data transmission.

The Feedback Node, which was implemented on the master PC, provides an interface to the client as shown in Figure 2. Whenever the subscriber of the LRA data receives new input from the Feedback Calculation Node, it is sent to the client as a JSON string. Simultaneously, the Feedback Node receives IMU data in the JSON format from the client, which is then decoded and published to the Orientation Node. In applications with robotic or virtual limbs, the Feedback Calculation Node could be fed with force data from the actuator that can be translated into vibration intensities, while the IMU data received by the Orientation Node could be used for control.

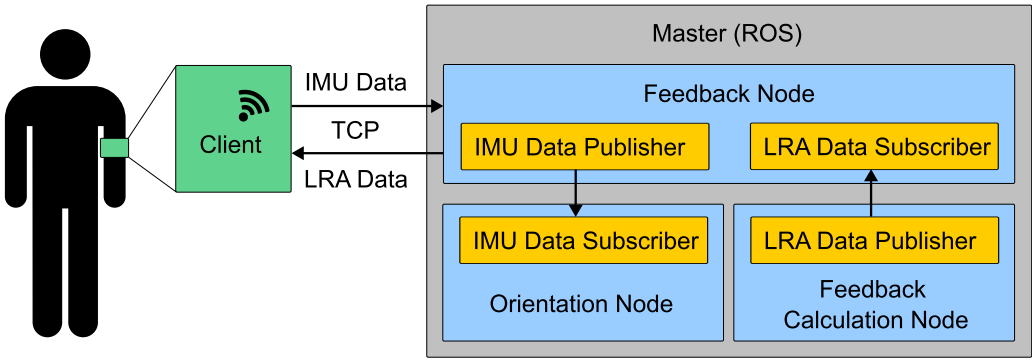

Figure 2. ROS interface on a master PC to communicate with the haptic feedback bracelet (client) allowing for bidirectional communication and broad compatibility. Vibration intensities are sent by a master PC to the client, which provides IMU data in exchange.

2.3. Mechanical Design of the Adjustable Bracelet

During the mechanical design of the haptic feedback bracelet, special emphasis was put on compactness and ease of use. The bracelet can be applied by the user, as the design of the bracelet ensures that the vibration modules are evenly distributed around the arm. The structure of the feedback bracelet is modular, consisting of up to five modules connected by flexible links as shown in Figure 3. However, the effective number of cues can be increased by making use of phantom tactile sensation [20]. Further, the feedback bracelet consists of two kinds of modules, a bigger main module containing the PCB, battery, force sensor, and an LRA, while the smaller modules only contain an LRA. The circumference of the bracelet is variable and ranges from 20 cm to 30 cm in its current configuration, thus being suitable to be worn on forearms and upper arms by the majority of people. The links are available in more sizes, covering an even wider range in circumference and the size of the links can be further adjusted using the CAD models from the publicly available repository (https://github.com/ASM-FAU/Haptic-Feedback-Armband, (accessed on 22 May 2024)) if needed.

Both the casing and the links were 3D printed using Fused Deposition Modeling. The casing was made from PLA due to its low cost and light weight, while the links were made from TPU due to its flexibility and durability. The vibration motors are oriented within the modules so that the vibration axis is orthogonal to the skin surface.

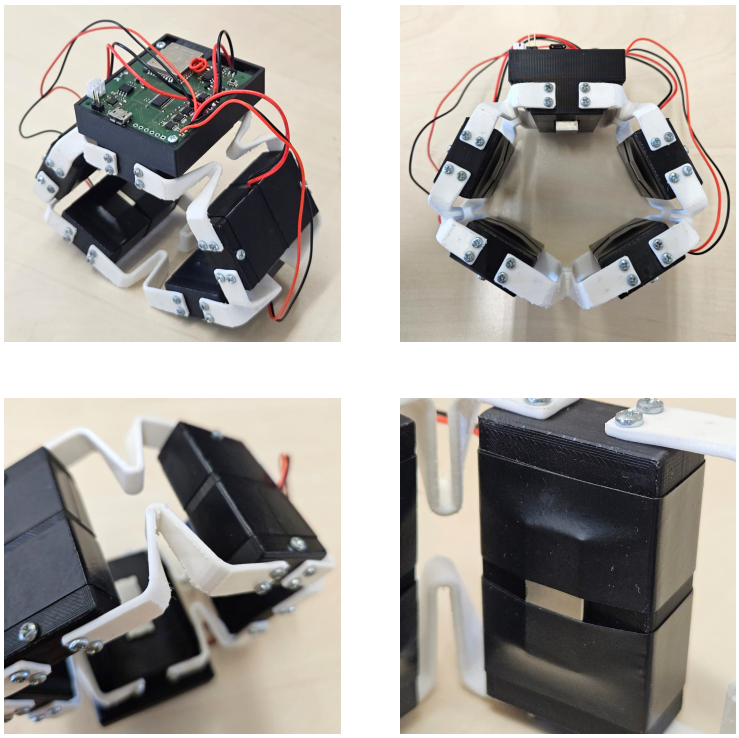

Figure 3. Pictures of the haptic feedback bracelet from multiple perspectives showing the modular and elastic design. The top left and top right pictures show a slanted and front view of the bracelet respectively. Flexible links connecting multiple vibration modules are shown in the lower left. The lower right picture shows a vibration module with tape to smoothen the edges of LRAs.

The main module is divided into two parts: the upper half accommodates the PCB and battery, while the lower half contains the vibration motor and FSR as shown in Figure 4. The vibration motor is placed at the bottom of the main module, fixed by the case to restrict any horizontal movements with enough clearance so the LRA can freely move along the vertical axis. The LRA protrudes the case by around 3 mm to ensure good skin contact with the user's arm. A plastic structure (force transmitter) is attached to the top of the LRA, which serves two purposes. When the bracelet is not worn, the edge of the protrusion of the force transmitter engages with the upper edge of the guidance structure for the LRA, preventing the vibration motor from falling out of the module. When the bracelet is worn, the force coming from the skin pushes the LRA and the attached force transmitter inward. At the top of the force transmitter is a cylindrical protrusion that then presses against the FSR sensor directly above it, effectively covering the active area of the FSR (see Figure 5 upper left) and thus allowing reliable force measurements that provide information about the fit of the bracelet. The FSR is supported by a plastic structure to provide a solid foundation for consistent force readings, also preventing any force from being transmitted to the battery above (see Figure 5 upper right and lower left). The upper half of the case, measuring 55 mm × 48.8 mm × 14 mm, contains four standoffs to enclose the battery and to mount the custom-designed PCB on top as shown in Figure 5. The red cables in the upper part of Figure 5 (lower right) fix an error in the initial design of the PCB. The circuit diagrams were corrected and are available in the online repository (https://github.com/ASM-FAU/Haptic-Feedback-Armband (accessed on 22 May 2024)).

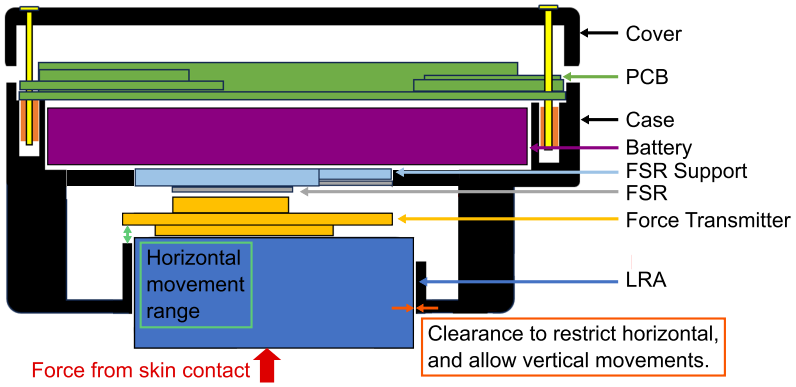

Figure 4. Schematic design of the main module of the haptic feedback bracelet, housing an LRA, FSR, battery, and PCB.

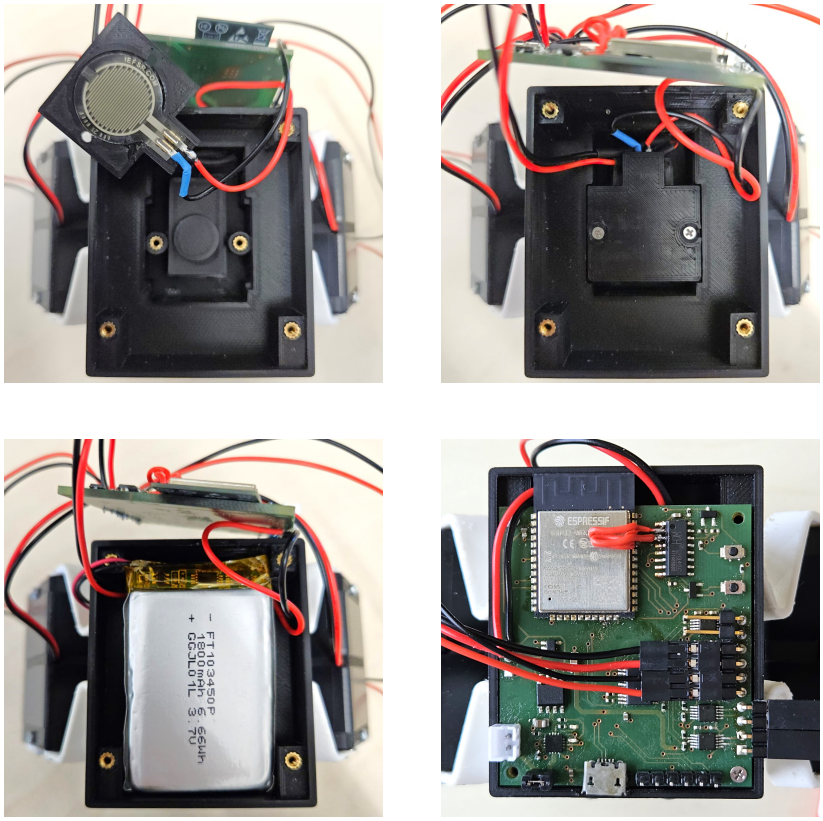

Figure 5. Pictures showing the structure and assembly of the main module containing an LRA, FSR, battery, and PCB. The force transmitter with cylindrical protrusion and the exposed FSR are shown on the upper left. The upper right shows the FSR support mounted to shield the battery from forces. The lower left picture shows the 1800 mAh lithium polymer battery secured by standoffs. The custom PCB being mounted on top of the battery is shown in the lower right picture.

The smaller modules measure 51 mm × 30 mm × 15.1 mm. They were designed to house a vibration motor only. Each module comprises a case and a lid, which can be firmly connected using M2 screws. The case was designed to hold the LRA by friction to prevent it from falling out of the module when not worn. A protrusion of the cover ensures that the LRA protrudes the case by 3 mm when worn assuring good skin contact as shown in Figure 6. A notch at the side of the case leaves room for the cables of the LRA to be connected to the respective pins on the PCB inside the main module. To smoothen the edges of the LRAs, the modules are wrapped in electric tape for a more comfortable wear as shown in Figure 3.

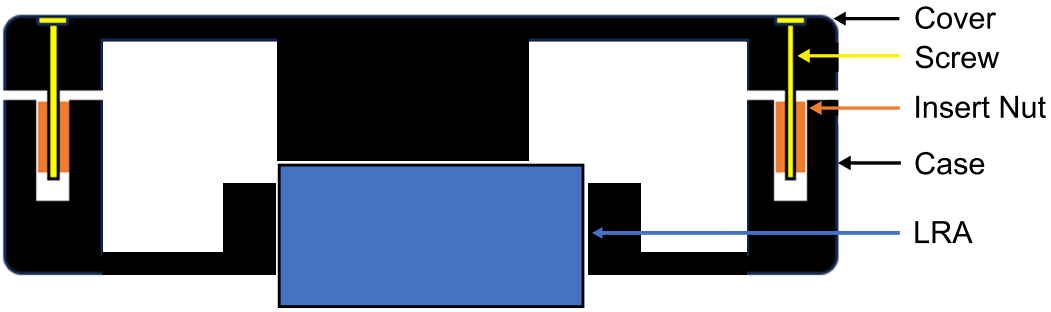

Figure 6. Schematic of a small module, housing an LRA only, which fits tightly in the case without the possibility to move.

3. Functional Tests and Evaluation

The purpose of the conducted experiments was to show the functionality and potential of the proposed haptic feedback device. The functional tests were conducted with a total of four healthy participants (of which two are authors of this paper) in their twenties and thirties. During the experiments, the participants wore the bracelet on the forearm as shown in Figure 7. The experiment was split into two parts, in both of which the participants were asked to estimate the vibration intensity levels generated by the haptic feedback bracelet on a predefined scale. For the first experiment, three different vibration intensity levels were defined. The lowest vibration intensity, 1, was defined as the lowest possible intensity that the LRAs can exert. The highest intensity, 3, was defined as the maximum possible vibration intensity by the LRAs. The medium intensity, 2, was set as the average value between these two extremes. In the second part, the vibration intensity range of the haptic feedback bracelet was divided into five levels, whereas Levels 1, 3, and 5 matched Levels 1, 2, and 3 of part one of the experiment, respectively. Intensity level 2 was then set between Levels 1 and 3, while Level 4 was set between Levels 3 and 5. In both parts of the experiment, the vibration intensity levels were played ten times each by all five LRAs simultaneously for five seconds in a random order. Before each part of the experiment, the participants were familiarized with the vibration intensity scale by playing each level three times in a known sequence.

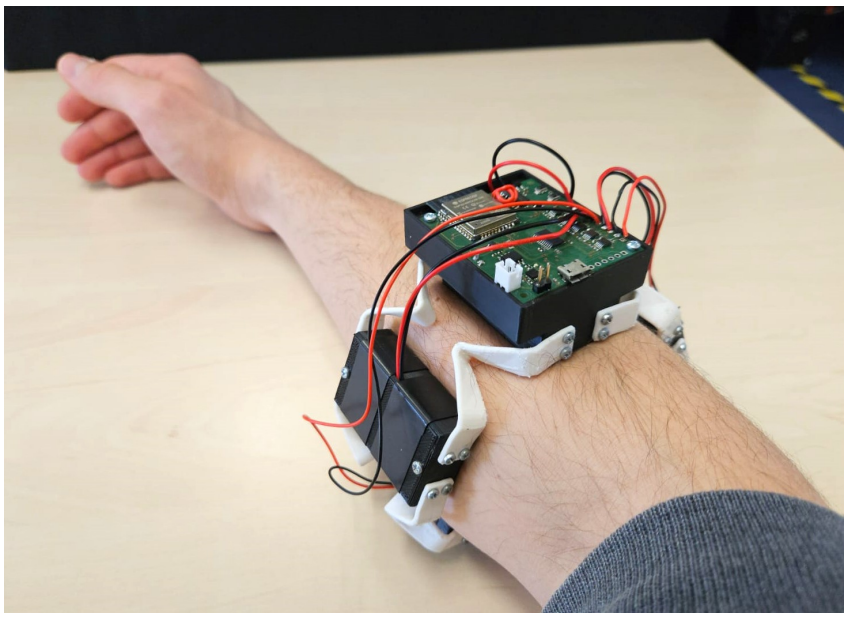

Figure 7. Experimental setup for the functional tests. Participants wore the bracelet on the forearm and were asked to estimate the different vibration intensities in a random order on a predefined scale.

The results of part one of the experiment in Figure 8 on the left show a high estimation accuracy across all vibration intensity levels. Level 1 was correctly estimated at 93%, Level 2 at 90%, and Level 3 at 80% accuracy. Misestimations did not surpass one intensity level. The average accuracy across all four participants was 88% with a standard deviation of 4.4%.

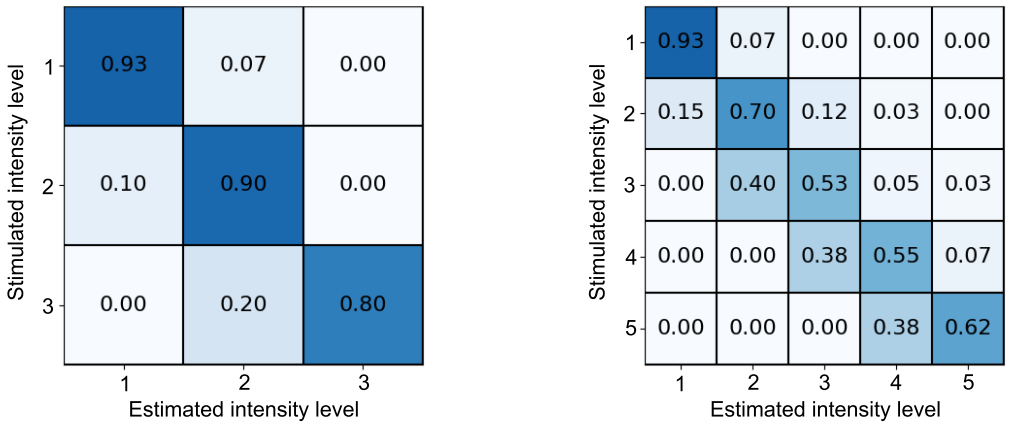

Figure 8. Confusion matrices for the estimation of different vibration intensity levels for both parts of the experiment averaged across all four participants. Part 1 (left): Estimating three vibration intensity levels with an average accuracy of 88%. Part 2 (right): Estimating five vibration intensity levels with an average accuracy of 67%.

While the results from part one of the experiment look promising, the accuracy in distinguishing five different vibration intensity levels across the same intensity range dropped significantly to only 67%, indicating poor performance at first glance. Additionally, accuracies between participants showed a much higher standard deviation of 11.1%. The analysis of the confusion matrix of the second part of the experiment in Figure 8 reveals that the low vibration intensity Levels 1 and 2 were correctly estimated with accuracies of 93% and 70%, respectively. However, the accuracy for Levels 3 to 5 only ranged from 53% to 62%, exhibiting a rather high error rate. Generally, misclassifications did not surpass one intensity level in the vast majority of cases, with a clear tendency to rate the perceived intensity lower as shown in Figure 8.

In part two of the experiment, it was observed that if an intensity level was falsely estimated, the subsequent value was also often misidentified by the offset to the true value by the previous estimation, leading to a low-absolute-vibration-intensity level estimation accuracy. The results might, however, still imply a higher relative vibration intensity-level estimation accuracy, which would not be impacted by this effect. To investigate this, the following adjustment was applied: Each time a level was estimated incorrectly, the difference was stored as an offset. If the randomly selected subsequent intensity level was misclassified by this offset, it was marked as correct, helping to account for consecutive errors, which were eliminated in the relative level estimation graph in Figure 9. This lead to a relative vibration intensity level estimation accuracy of 82% with a standard deviation of 6.2% across participants, which was much lower than the 11.1% standard deviation for absolute level estimation. This more consistent behavior can also be seen in the graph for relative level estimation of Figure 9, which shows a more linear behavior throughout the experiment.

The examination of the arithmetically averaged cumulative accuracy over the number of trials showed an increase in accuracy within the first 20 trials and stabilized at around 65%, which can be seen in Figure 10. This trend suggests a trainable recognition of the different vibration intensity levels.

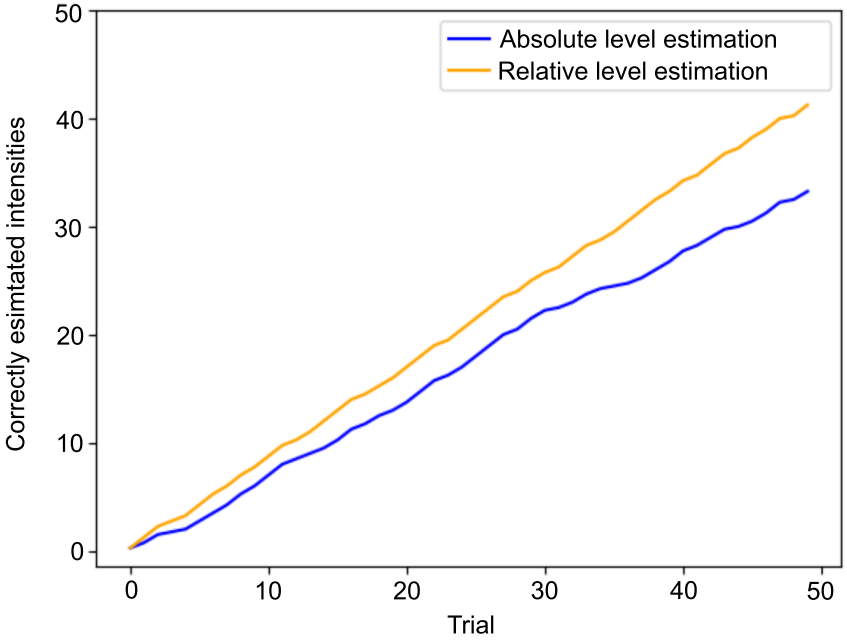

Figure 9. Average of correctly estimated absolute vibration intensity levels across all participants throughout the second part of the experiment represented by the blue line. The correctly estimated vibration intensity levels after offset adjustment are represented by the orange line, where intensity levels were rated in relation to the previously estimated vibration intensity level, indicating a relative vibration intensity level estimation accuracy of 82%.

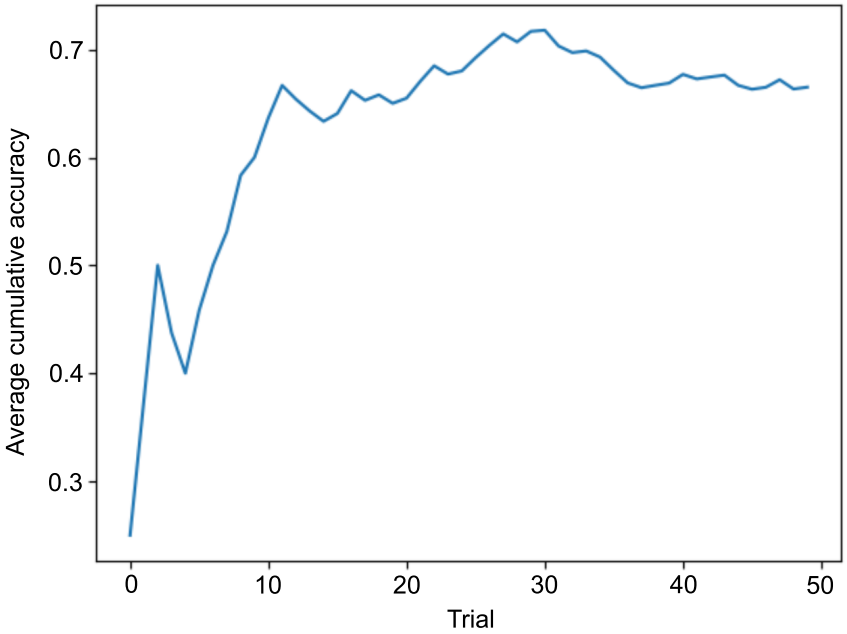

Figure 10. Arithmetically averaged cumulative vibration intensity level estimation accuracy over the number of trials, stabilizing at around 65% accuracy after the first 20 trials.

To evaluate the IMU's performance, we rotated the sensor using a motor equipped with a motion encoder. The rotation followed a sine wave pattern, spanning 90 degrees in both clockwise and counterclockwise directions from the initial position. Each sine wave cycle lasted 5 s, with four recorded cycles totaling 20 s duration. Figure 11 displays a graph of the data collected from both the encoder and the IMU. Due to processing and transmission delays, no absolute encoder timestamp is available. Accordingly, we synchronized the encoder and IMU data manually through relative timestamps to compare the signals but

did not consider latencies. The IMU data were converted from quaternions to Euler angles to allow for a direct comparison to the encoder data, which is considered as ground-truth data in this experiment. The IMU signal (blue line) followed the encoder signal (dashed red line) closely with some minor deviations in the sine-wave pattern. During the 20 s recording, the IMU showed no visible drift.

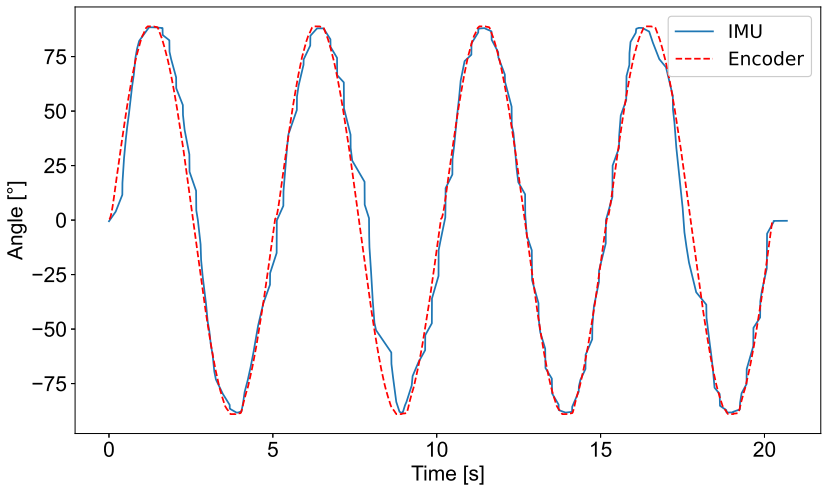

Figure 11. IMU and encoder angle readings over time from a sine wave motion. The rotation is induced by a motor rotating 90 degrees in each direction from the starting position for 20 s.

Finally, we conducted a small experiment with one participant to assess the functionality of the FSR inside the main module. The FSR output is dimensionless, ranging from 0 to 1, representing force values between 0.1 N and 10 N. Calibration can be employed to translate these FSR values into Newtons. In the experiment, the bracelet was worn on the forearm, as depicted in Figure 7. The participant was instructed to flex their forearm muscles at regular intervals. The graph in Figure 12 illustrates the FSR values over time, showing distinct spikes in force values above 0.70 when the forearm muscles are flexed compared to the relaxed state with values around 0.55.

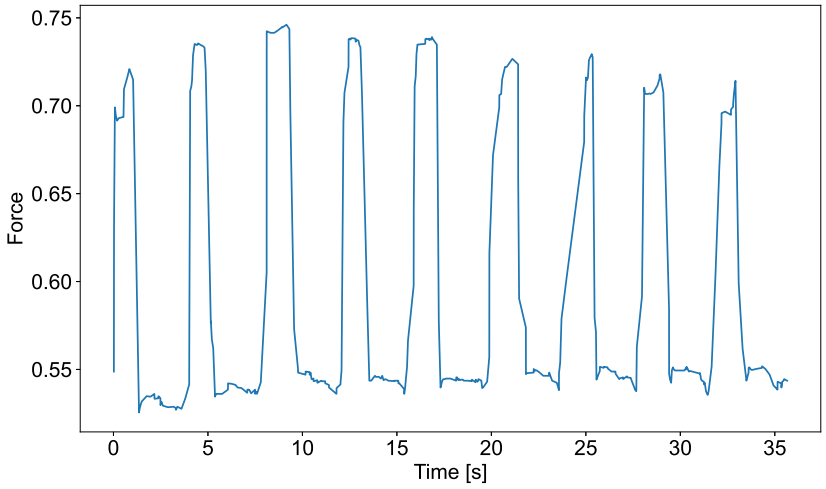

Figure 12. Force readings of the FSR over time from the haptic feedback bracelet worn on the forearm with regular intervals of muscle flexing. The values can range from 0 to 1 covering a force range of 0.1 N to 10 N according to the datasheet.

4. Discussion

Focusing on confirming functionality, we conducted our analyses with a limited number of participants. A deeper analysis of human–machine performance requires more extensive user studies. The absolute estimation of three different vibration intensity levels showed a high accuracy of 88%. While the accuracy of estimating absolute vibration intensities significantly dropped to 67% with five vibration intensity levels, the estimation of relative vibration intensity changes was again high with an accuracy of 82%. This behavior indicates difficulties for the participants to estimate absolute vibration intensities, but good performance in the estimation of relative changes in vibration intensity. This is in line with the results of the study by Hatzfeld et al. [34] that showed high sensitivity to differential vibration in the fingertip at a frequency of 160 Hz. For the experiments, the vibration intensity levels were distributed in equal intervals on the intensity scale. The confusion matrix in Figure 8 showed lower estimation accuracies for vibration intensity Levels 3 to 5 compared to Levels 1 and 2. A redistribution of vibration intensity levels towards smaller intervals between Levels 1 and 2 and bigger intervals between Levels 2 to 5 could accomplish a more even estimation accuracy across vibration intensity levels.

During the experiments, it was noticed that the vibration from the LRA of the main module was perceived as much stronger than the ones of the smaller modules even though the LRAs were identical. The four LRAs in the smaller modules were rigidly integrated without any freedom of movement in each module, while the LRA inside the main module could move along the vibration axis to enable the transmission of force to the force-sensitive resistor above. The rigid integration of the LRAs into the smaller modules might dampen the vibration. Further, the additional weight of the main module due to the included battery and PCB can alter the vibration compared to the smaller modules. Revising the placement of the motors and providing a uniform attachment could ensure that the vibration motors contribute equally to the overall perception. These changes could contribute to optimizing the performance and accuracy of the system, expanding its applicability to a larger user base and ultimately increasing the system's potential for practical applications.

The test with the IMU in Figure 11 shows minimal deviations from the encoder data and no visible drift, indicating satisfactory performance. Further, the results of the experiment with the force-sensitive resistor in Figure 12 show its suitability for intent detection through the distinct spikes in force values when flexing the forearm muscle. Further, the sensor readings during the relaxed state are consistent, around the same value throughout the experiment, indicating good reliability. Fischer et al. [28] examined a shift in perceived vibration intensity based on the tightness of a haptic feedback bracelet. Adjusting the vibration intensities depending on the tightness of the bracelet should help to provide a consistently perceived vibration across users with different arm circumferences. Although this is already partially accounted for by the elastic design of the bracelet, the integration of a force-sensitive resistor into the haptic feedback bracelet allows for studying the connection more closely and could have a meaningful impact on the understanding of haptics and the design of future haptic feedback devices.

5. Conclusions

The presented haptic feedback bracelet combines sensors with particularly strong vibration motors, which increase the range of different vibration intensity levels. The integration of an IMU to gather motion data can be useful to control robotic and virtual limbs, but could also be helpful in many other instances that require simultaneous motion capturing and haptic feedback in a single device. A custom PCB was designed to account for the high current requirement of the five LRAs. The use of an efficient microcontroller with two cores decreased latency, leading to a responsive operation. Moreover, the integration of most circuit components onto the board enabled a compact design. The integrated battery and WiFi module allowed for complete wireless operation, making the device wearable and enabling communication through an ROS interface. Additionally, the ROS interface allowed for easy integration with other existing systems, and by making all software and

hardware (including all 3D models and circuit diagrams) publicly available in a GitHub repository (https://github.com/ASM-FAU/Haptic-Feedback-Armband (accessed on 22 May 2024)), the platform can be further improved and used by the research community.

Future studies should include objective measurements of the different vibration intensity levels by a high-quality vibrometer. This could facilitate comparisons to other haptic feedback devices and would provide deeper insight into the perception of haptic feedback. Furthermore, future research could test the proposed bidirectional haptic feedback bracelet in specific interactive applications to explore potential benefits in performance and user experience. We expect such systems to facilitate deeper analysis of human–machine interfaces and to improve the intuitiveness and reliability of interaction.

Author Contributions: Conceptualization, D.A., A.D. and P.B.; methodology, J.K., D.A., Z.H. and A.D.; software, J.K.; validation, D.A., A.D. and P.B.; formal analysis, J.K. and D.A.; investigation, J.K. and D.A.; resources, D.A. and P.B.; data curation, J.K. and D.A.; writing—original draft preparation, J.K., D.A. and Z.H.; writing—review and editing, D.A., A.D. and P.B.; visualization, J.K., D.A. and Z.H.; supervision, P.B.; project administration, D.A., A.D. and P.B.; funding acquisition, P.B. All authors have read and agreed to the published version of the manuscript.

Funding: This research was funded by the German Research Foundation (DFG) grant number BE 5729/16-1.

Institutional Review Board Statement: Not applicable.

Informed Consent Statement: Informed consent was obtained from all subjects involved in the functional tests.

Data Availability Statement: All the data contains in the article.

Acknowledgments: The authors would like to thank Florian Warko who assisted in the design and manufacturing of the PCB.

Conflicts of Interest: The authors declare no conflicts of interest.

Abbreviations

The following abbreviations are used in this manuscript:

LRA	Linear Resonant Actuator
DC	Direct Current
IMU	Inertial Measurement Unit
ROS	Robot Operating System
PCB	Printed Circuit Board
SMD	Surface-Mounted Device
FSR	Force-Sensitive Resistor
TCP	Transmission Control Protocol

References

1. MacKenzie, I.S. *Human-Computer Interaction: An Empirical Research Perspective*; Morgan Kaufmann Publishers Inc.: San Francisco, CA, USA, 2013.
2. Pinardi, M.; Longo, M.R.; Formica, D.; Strbac, M.; Mehring, C.; Burdet, E.; Di Pino, G. Impact of supplementary sensory feedback on the control and embodiment in human movement augmentation. *Commun. Eng.* **2023**, *2*, 64. [CrossRef]
3. Thomas, N.; Miller, A.J.; Ayaz, H.; Brown, J.D. Haptic shared control improves neural efficiency during myoelectric prosthesis use. *Sci. Rep.* **2023**, *13*, 484. [CrossRef] [PubMed]
4. Huynh, V.; Bekrater-Bodmann, R.; Fröhner, J.; Vogt, J.; Beckerle, P. Robotic hand illusion with tactile feedback: Unravelling the relative contribution of visuotactile and visuomotor input to the representation of body parts in space. *PLoS ONE* **2019**, *14*, e0210058. [CrossRef]
5. Dietrich, C.; Walter-walsh, K.; Preißler, S.; Hofmann, G.O.; Witte, O.W.; Miltner, W.H.R.; Weiss, T. Neuroscience Letters Sensory feedback prosthesis reduces phantom limb pain: Proof of a principle. *Neurosci. Lett.* **2012**, *507*, 97–100. [CrossRef] [PubMed]
6. Antfolk, C.; D'Alonzo, M.; Rosén, B.; Lundborg, G.; Sebelius, F.; Cipriani, C. Sensory feedback in upper limb prosthetics. *Expert Rev. Med. Devices* **2013**, *10*, 45–54. [CrossRef]

7. Mounier, S. *Entwicklung Einer Realitätsnahen Kraftrückkopplung bei Fluidisch Betriebenen Handprothesen*; Forschungszentrum Karlsruhe: Karlsruhe, Germany, 2004.
8. Fitch, G.M. Driver Comprehension of Integrated Collision Avoidance System Alerts Presented through a Haptic Driver Seat. Ph.D. Thesis, Virginia Tech, Blacksburg, VA, USA, 2008.
9. Nemah, M.N.; Low, C.Y.; Aldulaymi, O.H.; Ong, P.; Ismail, A.E.; Qasim, A.A. A Review of Non-Invasive Haptic Feedback stimulation Techniques for Upper Extremity Prostheses. *Int. J. Integr. Eng.* **2019**,*11*, 280–290. [CrossRef]
10. Svensson, P.; Wijk, U.; Björkman, A.; Antfolk, C. A review of invasive and non-invasive sensory feedback in upper limb prostheses. *Expert Rev. Med. Devices* **2017**, *14*, 439–447. [CrossRef]
11. Dahiya, R.; Metta, G.; Valle, M.; Sandini, G. Tactile Sensing—From Humans to Humanoids. *IEEE Trans. Robot.* **2010**, *26*, 1–20. [CrossRef]
12. Antfolk, C.; Balkenius, C.; Lundborg, G.; Rosén, B.; Sebelius, F. Design and technical construction of a tactile display for sensory feedback in a hand prosthesis system. *Biomed. Eng. Online* **2010**, *9*, 50. [CrossRef] [PubMed]
13. Wang, D.; Zhao, K.; Yuan, Y.; Wang, Z.; Zong, H.; Zhang, X.; Liang, J. Fabrication and characterization of a microscale piezoelectric vibrator based on electrohydrodynamic jet printed PZT thick film. *Micromachines* **2021**, *12*, 524. [CrossRef] [PubMed]
14. Abd, M.A.; Bornstein, M.; Tognoli, E.; Engeberg, E.D. Armband with soft robotic actuators and vibrotactile stimulators for bimodal haptic feedback from a dexterous artificial hand. In Proceedings of the 2018 IEEE/ASME International Conference on Advanced Intelligent Mechatronics (AIM), Auckland, New Zealand, 9–12 July 2018; pp. 13–20.
15. Berkovic, A.; Laganier, C.; Chappell, D.; Nanayakkara, T.; Kormushev, P.; Bello, F.; Rojas, N. A Multi-modal Haptic Armband for Finger-Level Sensory Feedback from a Prosthetic Hand. In Proceedings of the International Conference on Human Haptic Sensing and Touch Enabled Computer Applications, Hamburg, Germany, 22–25 May 2022; Springer: Berlin/Heidelberg, Germany, 2022; pp. 138–146.
16. Gao, S.; Yan, S.; Zhao, H.; Nathan, A. *Touch-Based Human-Machine Interaction: Principles and Applications*, 1st ed.; Springer eBook Collection, Springer International Publishing and Imprint Springer: Cham, Switzerland, 2021. [CrossRef]
17. Gunther, E.E.L. Skinscape: A tool for Composition in the Tactile Modality. Ph.D. Thesis, Massachusetts Institute of Technology, Cambridge, MA, USA, 2001.
18. Kaczmarek, K.A.; Webster, J.G.; Bach-y Rita, P.; Tompkins, W.J. Electrotactile and vibrotactile displays for sensory substitution systems. *IEEE Trans. Biomed. Eng.* **1991**, *38*, 1–16. [CrossRef]
19. Bimbo, J.; Pacchierotti, C.; Aggravi, M.; Tsagarakis, N.; Prattichizzo, D. Teleoperation in cluttered environments using wearable haptic feedback. In Proceedings of the IEEE/RSJ International Conference on Intelligent Robots and Systems, Vancouver, BC, Canada, 24–28 September 2017; Conference Digest; IEEE: Piscataway, NJ, USA, 2017.
20. Seiler, J.; Schäfer, N.; Latsch, B.; Chadda, R.; Hessinger, M.; Beckerle, P.; Kupnik, M. Wearable Vibrotactile Interface Using Phantom Tactile Sensation for Human-Robot Interaction. In *Proceedings of the Haptics: Science, Technology, Applications*; Nisky, I., Hartcher-O'Brien, J., Wiertlewski, M., Smeets, J., Eds.; Springer International Publishing: Cham, Switzerland, 2020; pp. 380–388.
21. Visconti, P.; Gaetani, F.; Zappatore, G.A.; Primiceri, P. Technical features and functionalities of Myo armband: An overview on related literature and advanced applications of myoelectric armbands mainly focused on arm prostheses. *Int. J. Smart Sens. Intell. Syst.* **2018**, *11*, 1–25. [CrossRef]
22. Schätzle, S.; Hulin, T.; Pleintinger, B. VibroTac S: An electronic assistive device for blind and visually impaired people to avoid collisions. In Proceedings of the Human Systems Engineering and Design: Proceedings of the 1st International Conference on Human Systems Engineering and Design (IHSED2018): Future Trends and Applications, CHU-Université de Reims Champagne-Ardenne, France, 25–27 October 2018; Springer: Berlin/Heidelberg, Germany, 2019; pp. 613–619.
23. Aug, A.; Slepyan, A.; Levenshus, E.; Thakor, N. Haptic Touch: A retrofittable tactile sensing glove and haptic feedback armband for scalable and robust sensory feedback. In Proceedings of the 2022 9th IEEE RAS/EMBS International Conference for Biomedical Robotics and Biomechatronics (BioRob), Seoul, Republic of Korea, 21–24 August 2022; pp. 1–6.
24. Clark, J.P.; Lentini, G.; Barontini, F.; Catalano, M.G.; Bianchi, M.; O'Malley, M.K. On the role of wearable haptics for force feedback in teleimpedance control for dual-arm robotic teleoperation. In Proceedings of the 2019 International Conference on Robotics and Automation (ICRA), Montreal, QC, Canada, 20–24 May 2019; pp. 5187–5193.
25. Wang, M.; Bulger, M.; Dai, Y.; Noël, K.; Axon, C.; Brandenberger, A.; Fay, S.; Gao, Z.; Gilmer, S.; Hamdan, J.; et al. A 3D-Printed, adjustable armband for electromyography-based finger movement classification with haptic feedback. In Proceedings of the 2020 IEEE International Conference on Systems, Man, and Cybernetics (SMC), Toronto, ON, Canada, 11–14 October 2020; pp. 3460–3465.
26. Fang, Y.; Guo, W.; Sheng, X. Toward a Wireless Wearable System for Bidirectional Human-Machine Interface With Gesture Recognition and Vibration Feedback. *IEEE Sens. J.* **2022**, *22*, 9462–9472. [CrossRef]
27. Feng, K.; Lei, M.; Wang, X.; Zhou, B.; Xu, Q. A Flexible Bidirectional Interface with Integrated Multimodal Sensing and Haptic Feedback for Closed-Loop Human–Machine Interaction. *Adv. Intell. Syst.* **2023**, *5*, 2300291. [CrossRef]
28. Fischer, J.; Andreas, D.; Dwivedi, A.; Beckerle, P. The Contribution of Sensors to Haptic Feedback in Robotic Hand Control and Teleoperation. In *Sensor and Measurement Science International*; AMA Association for Sensors and Measurement: Wunstorf, Germany, 2023; pp. 221–222. [CrossRef]

29. Tang, A.M.; Chung, M.; Dong, K.R.; Bahwere, P.; Bose, K.; Chakraborty, R.; Charlton, K.; Das, P.; Ghosh, M.; Hossain, M.I.; et al. Determining a global mid-upper arm circumference cut-off to assess underweight in adults (men and non-pregnant women). *Public Health Nutr.* **2020**, *23*, 3104–3113. [CrossRef] [PubMed]
30. Anakwe, R.; Huntley, J.; McEachan, J.E. Grip strength and forearm circumference in a healthy population. *J. Hand Surg. (Eur. Vol.* **2007**, *32*, 203–209. [CrossRef] [PubMed]
31. Østlie, K.; Lesjø, I.M.; Franklin, R.J.; Garfelt, B.; Skjeldal, O.H.; Magnus, P. Prosthesis rejection in acquired major upper-limb amputees: a population-based survey. *Disabil. Rehabil. Assist. Technol.* **2012**, *7*, 294–303.
32. Attig, C.; Rauh, N.; Franke, T.; Krems, J.F. System latency guidelines then and now–is zero latency really considered necessary? In Proceedings of the Engineering Psychology and Cognitive Ergonomics: Cognition and Design: 14th International Conference, EPCE 2017, Held as Part of HCI International 2017, Vancouver, BC, Canada, 9–14 July 2017; Part II 14; Springer: Berlin/Heidelberg, Germany, 2017; pp. 3–14.
33. Kangas, J.; Rantala, J.; Akkil, D.; Isokoski, P.; Majaranta, P.; Raisamo, R. Delayed Haptic Feedback to Gaze Gestures. In *Proceedings of the Haptics: Neuroscience, Devices, Modeling, and Applications*; Auvray, M., Duriez, C., Eds.; Springer: Berlin/Heidelberg, Germany, 2014; pp. 25–31.
34. Hatzfeld, C.; Cao, S.; Kupnik, M.; Werthschutzky, R. Vibrotactile Force Perception—Absolute and Differential Thresholds and External Influences. *IEEE Trans. Haptics* **2016**, *9*, 586–597. [CrossRef] [PubMed]